Design and Construction of a Single-Axis Linear Motor

Sara Davidova
Electrical Engineering - Stanford University
Email: sarinka@stanford.edu

Maisam Pyarali
Electrical Engineering - Stanford University
Email: maisam@stanford.edu

***Abstract*—The goal of this project was to design, build, and validate a modular design of a single-axis linear motor, capable of moving a load in a horizontal plane. The motor was constructed to slide on a linear rail equipped with a Halbach magnetic array. A carriage sliding over the array was fastened by linear bearings and carried two sets of three coils, one per each phase of the motor. Hall effect sensors were suspended inside the coil bobbins, and were used by an ODrive as a source of position measurements. According to an FEMM simulation, the design would generate about 3N of force when a current of 0.5A was commutated across the coils. This report discusses in detail the design, construction, and validation of the system.**

I. Introduction

The first linear motor was invented in the late 1940s by Dr. Eric Laithwaite, nearly 200 years after the first rotary motor [1]. This project has been inspired by the relative novelty of the motor, and the continuously growing literature exploring and validating different designs for various applications.

Essentially, a linear motor can be understood as an unrolled rotary motor, where the rotor slides horizontally along a rail of magnets, rather than spinning inside a stator. Linear motors span many different architectures, including flat, planar, or tubular, usually implemented as brushless motors [2].

Standard single-axis low-acceleration linear motors are used for transportation applications, for example in maglev trains. High-acceleration linear-motors are more common for moving loads of lower mass for high-precision industrial applications such as IC manufacturing or general automation. Recently, the linear architecture has been used for novel electricity generators, such as the Mainspring linear generator which periodically compresses a gas chamber to incite a low-temperature spatially-uniform fuel combustion, which in turn pushes on the pistons to generate electric current [3].

II. Specification

	Desired specification	Actual characteristics
Travel distance	0.3m	0.28m
Speed	0.25m/s	0.28m/s
Mass of load	1 kg	1.051kg* (0.834g carriage, 0.217 weight)

Fig. 1. Design Specifications (*Friction Load + Hanging Load)

The main purpose of the system was to position a certain load on specific x coordinates reachable by the motor. Since the precision of the motor depends less on the mechanical and electromagnetic design, and more on the quality of the encoding mechanism and the driver, no precision specifications were set within the scope of the project. Due to time constraints, no harsh efficiency specifications or dynamic response specifications were imposed either.

III. Architecture

Two different architectures were considered: a flat and a U-channel linear motor. A flat architecture is composed of a rail of magnets above which slides a set of coils. The coils are usually attached to a carriage which moves back and forth on the rails while maintaining contact via a set of linear bearings [4]. Unlike a flat architecture, a U-channel motor, where the coils slide in a channel between two magnet arrays, provides a stronger and more uniform magnetic field due to the presence of permanent magnets on both sides of the traveling electromagnet. The structure also lowers magnetic flux leakage, and improves safety since all moving parts are contained within the channel. However, a drawback is that the narrow channel impedes convective heat sinking compared to the flat architecture because the coils slide in a confined space [2]. Because the design was not going to be optimized for maximum efficiency, its thermal characteristics would likely be the limiting factor to its performance. Due to this consideration, the flat architecture was selected, and a Halbach magnet array was employed to make sure the magnetic field would not suffer significantly compared to the U-channel alternative.

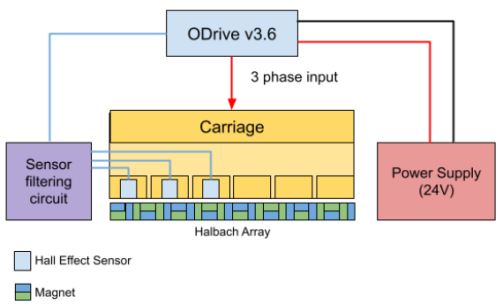

Fig. 2. Block Diagram of the Proposed Single-Axis Linear Motor System

IV. Electromagnetic Design

The key components of the electromagnetic system include:

1) **24V Power supply:** This power supply powers the drive, which uses it for its internal low voltage electronics, and converts it into a three phase sine wave driving the motor.
2) **ODrive v3.6:** The ODrive interfaces between the computer terminal and the motor. It is used to control the motor by providing current commutation, as well as receive encoder feedback to adjust the position of the motor as needed.
3) **Magnetic rail:** A set of permanent magnets in a Halbach array interacts with the coils and produces horizontal force.
4) **Coils:** Three coils (each composed of two windings) wired in a wye configuration interact with the magnets and propel the carriage.
5) **Hall effect sensors:** Three hall effect sensors suspended inside the coil bobbins create an encoding mechanism and interface with the ODrive to provide position measurements.

A simple Halbach array was composed of axially-polarized neodymium magnets of square cross-section, made out of strong magnetic material N-48. Thanks to the Halbach array channeling the magnetic flux towards the coils, the project was able to avoid the use of iron cores. Although the efficiency might suffer due to the lack of material with high magnetic permeability, an ironless design prevents cogging, and therefore enables smooth movement [5]. Two sets of three coils (one for each phase) were used, maximizing the force generated, without exceeding the size of the carriage. Each set was placed over 2 magnetic phases of the Halbach array, which was made to rotate in a counterclockwise manner, canceling the downward field and intensifying the upward field (see Figure (2) and (3)).

Approximately $2 - 4A/mm^2$ of current could theoretically be passed through the wire. Although the coils were not air cooled, the motor would only be in operation for very brief periods of time, so a maximum of $4A/mm^2$ was selected.

The closest the coils could lie above the magnet array was 2mm (accounting for 1mm of bobbin thickness and 1 mm of air to avoid friction). At this distance, and with the x and y dimensions of the coil determined by the array, the optimal coil height was identified to be 1.4cm. Bobbins dimensioned for this size allowed about 200 windings per coil, which translated to a 40% packing factor. A simulation was carried out in FEMM with the above-described characteristics.

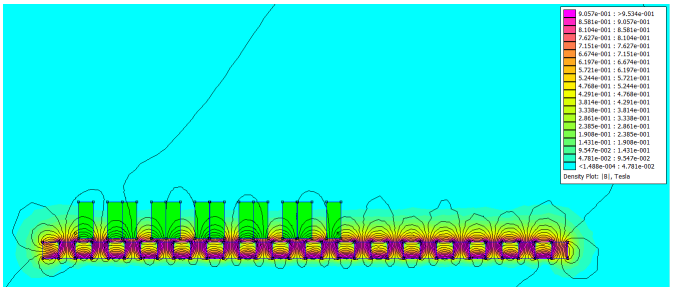

Fig. 3. FEMM Force Calculation with Two Sets of 0.564x1.4x2.54cm Coils Positioned 2mm above Array

The expected force was calculated by integrating the Lorentz force over the total cross-sectional areas of the coils during an exemplary state of trapezoidal current commutation. According to the simulation, a force of 3.06N would be generated.

The hall effect sensors would be mounted inside the coil bobbins. At 5mm from the array, the B-field the sensors would see has been simulated to vary between -0.3 to 0.3 Tesla, which is well above the resolution of 2.75mTpp, but also below the saturation level of 0.4 Tesla. The figure below shows the simulated magnetic field variation as the sensor travels over 4 magnetic rotations, corresponding to 16 magnets.

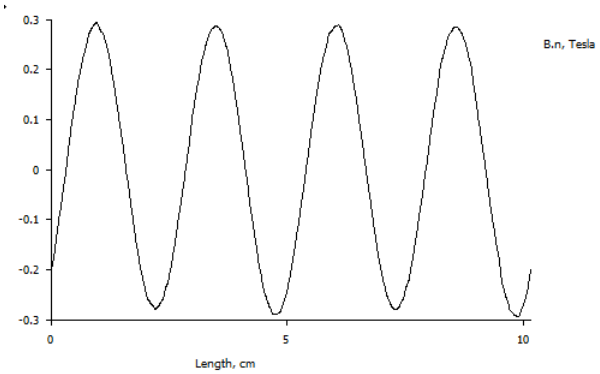

Fig. 4. Normal B-field 5mm above Halbach Array

Positioning the hall effect sensors inside the bobbins allowed them to be spaced apart exactly the same distance as the coil phases. This way, at least one of the hall effect sensors would trigger during each commutation transition, if trapezoidal commutation is employed, and the hall effect sensors should seamlessly interface with the ODrive in “hall sensor mode”. The output of the hall effect sensors was connected to a filtering circuit as recommended by the datasheet, see Figure (5). The filtered output was then fed into the Odrive hall effect encoder inputs.

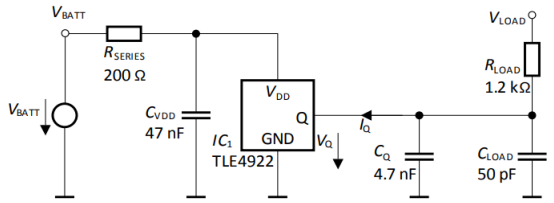

Fig. 5. Application Circuit for TLE4922 as Illustrated in the Datasheet

The thinnest available enameled wire - 26 AWG - was used since it allowed for a satisfactory packing factor due to ease of winding. The wire had a cross-sectional area of $0.129mm^2$, therefore a maximum current of 0.5A could be passed through. The wires were soldered to allow for connecting pairs of coils appertaining to the same phase, and creating a WYE connection in the middle.

V. Mechanical Design

While designing the linear motor, the use of commercially available components was prioritized. For more complex geometries like the coil bobbin, original designs were 3D printed.

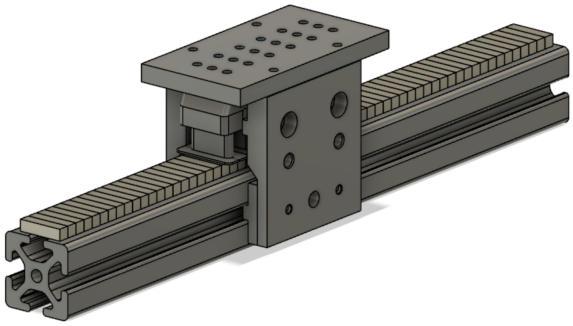

Fig. 6. Full CAD Rendering of Linear Motor

For the base of the design the standard 40 series 80/20 T-rail was used. 44 pieces of 25.4 x 6.35 x 6.35mm N48 neodymium magnets were placed on the bed to give a total linear range of 28cm. Using the sizes of the bed and the magnets as constraints, the bobbin width of 16.92mm was chosen.

To support the six electromagnets, a multipurpose 6061 aluminum block was ordered and cut to the calculated 11.85 cm. Holes were drilled into the aluminum block using a vertical mill at the measured positions and the bobbins were screwed in using 10-32 screws. As seen in figure 6 and 7, the bobbins and aluminum block had matching hole profiles to allow for easy matching and fitting.

An additional channel was extruded in the bobbin and drilled into the aluminum block to pass the coil wires and the wires connected to the terminals of the hall effect sensors. Finally the aluminum block was supported by two 40 series 80/20 uni-bearings. These served two purposes, to attach the coils and to slide the carriage along the T-rail.

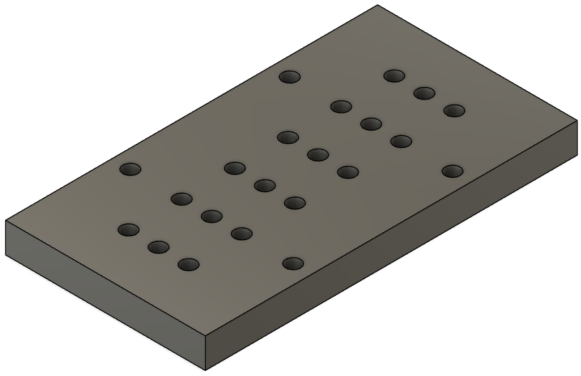

Fig. 7. Aluminum Support Block

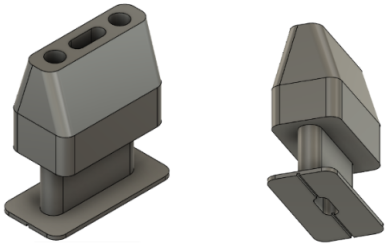

Fig. 8. Coil Bobbin

A BOM of the materials used is attached below as well as linked to the submission files.

Item	Quantity
25.4x6.35x6.35mm N48 neodym magnets	44
40 series 80/20 T-rail - 40cm	1
40 series 80/20 single short unibearing	2
Power supply (12V to 24V)	1
Hall effect sensors 0.4T	3
26AWG wire, 5m	1
Cable chain - 40cm	1
ODrive V3.6	1
40 series 80/20 Rubber door seal - 40cm	1
JB Weld	1
Multipurpose 6061 Aluminum Block (3/8" Thick x 2-1/2" Wide)	1
Black-Oxide Alloy Steel Socket Head Screw (10-32 Thread Size, 11/16" Long)	16
Tap for 10-32 Size Insert	1
10-32 Right-Hand Thread Helical Insert	4

Fig. 9. Bill of Materials

VI. Construction

There were three crucial steps in the construction process. Firstly, the magnetic array had to be assembled. Due to the choice of high grade magnets, the forces that had to be overcome in that process were considerable, so magnets had to be held in place using a steel plate. First the magnets were labeled with N-S marks, then they were ordered with the correct rotation but upside down on a piece of steel. JB weld was applied on the rail and the piece of steel was clamped to the rail with the magnets facing the rail. After letting them cure for 24 hours, the steel plate was pulled away, leaving the assembled array.

Fig. 10. Magnets on a Steel Plate Clamped to Rail to let JB Weld Cure

Next, the coils were wound. There were exactly 200 windings per bobbin, and the ends of the wires were fed through the designed channels and the extrusions in the bobbin toward the aluminum plate. Hall effect sensors were installed inside the extrusions on the first three coils. Due to the axis of measurement, which lies perpendicular to the sensor's body, the hall effect sensors had to be bent to lie parallel with the Halbach array. Coils were screwed to the aluminum plate, the phases were properly soldered together, and the wires from those phases and the hall effect sensors were fed to the ODrive through the cable chain. An additional filtering circuit necessary for the correct functioning of the hall effect sensors was constructed on an adjacent breadboard. The ODrive was configured for a current limit of 0.5A and 11 pole pairs, and was set to hall effect sensor mode (for full configuration command list, see appended file). The final setup can be seen on Figure (11).

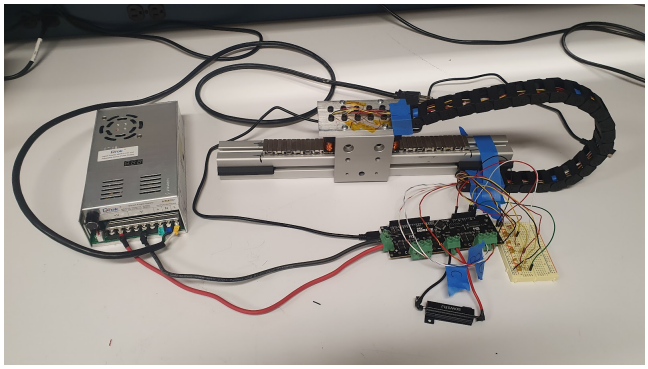

Fig. 11. Complete System Setup

VII. Validation

Complete control of the linear motor was not achieved, because of time constraints and issues with the ODrive controller. However, the motor was set into motion. This was achieved by running the ODrive configuration sequence. Unfortunately, the motor would only move in one direction, and would bump into the rubber seal multiple times before stopping. A thermal camera was used to monitor temperature increase in the different motor parts to ensure safe operations. Because the motor only sustained about 2 seconds of movement due to being run in the configuration settings, there was no observable increase (0.1°C) in temperature. The speed reached during this configuration sequence (likely not the fastest the motor is able to run) was 0.28m/s. To compare the performance with the FEMM simulation, force was measured by attaching a string with a weight hanging from the side of the table, and seeing whether the carriage could sustain motion. The heaviest weight that the carriage was able to support in a sustained manner was 156g. With a heavier weight, 217g, the carriage was able to generate the force momentarily, but did not sustain it. Considering that even in the case of unsustained motion, the motor must have been exerting significant energy at overcoming friction on top of lifting the weight, the simulated force was well within 1N of the actual force.

A significant issue that appeared during the construction was that an incorrect axis of measurement was assumed for the hall effect sensors - instead of measuring in line with the pins of the sensor, they measured perpendicular to the body of the sensor. This assumption caused an incorrect dimensioning of the coil extrusion, which was too narrow to allow for a hall effect sensor to lie inside horizontally. Therefore, the hall effect sensors were only tilted slightly, and not uniformly. This caused a significant issue in their performance, because there was a phase shift in the magnetic fields they were subjected to. Figure 10 and 11 show the difference in the perpendicular and tangential B-field above the magnetic array. It can be observed that measuring under a different angle causes a phase shift in the reading.

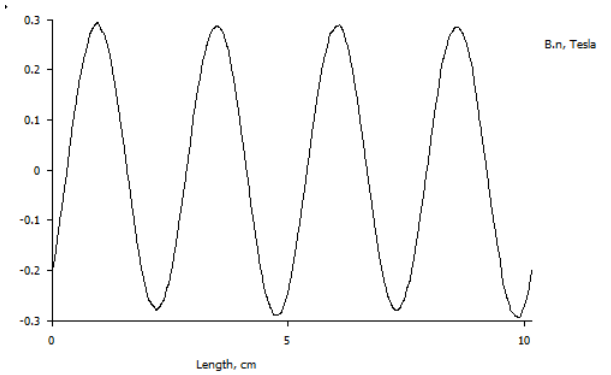

Fig. 12. Perpendicular B-field 5mm above Halbach Array

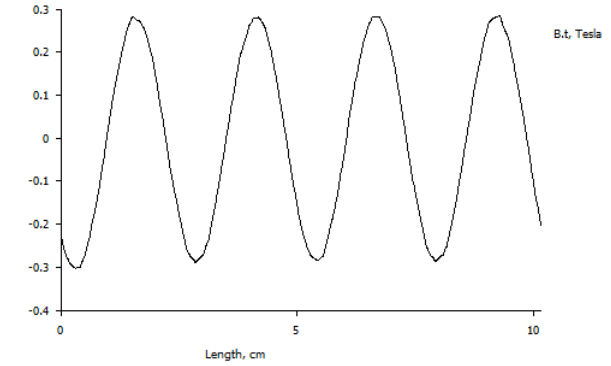

Fig. 13. Tangential B-field at 5mm from Magnetic Array

Because of the varying phase shifts, the hall effect sensors did not trigger as expected, and therefore did not align with the desired current commutation. Figures (14) and (15) show the output of the sensors during motion. Two sensors are phase shifted such that they essentially act as a quadrature encoder. The last sensor is shifted such that it perfectly aligns with one of the first two. Although it would be possible to experiment with a quadrature encoder mode on the ODrive, the current positioning of the hall effect sensors prevented a good performance in hall effect mode.

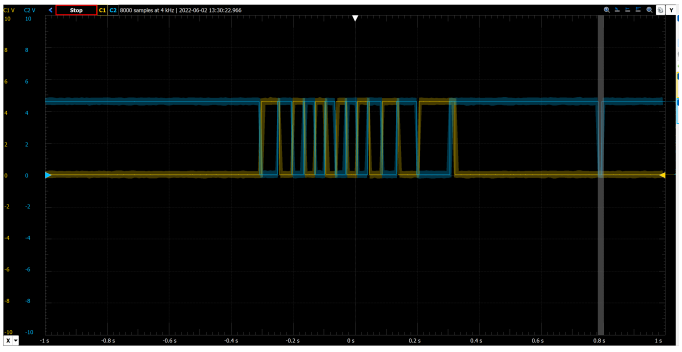

Fig. 14. Hall Effect Sensors Outputs for Phases A and B

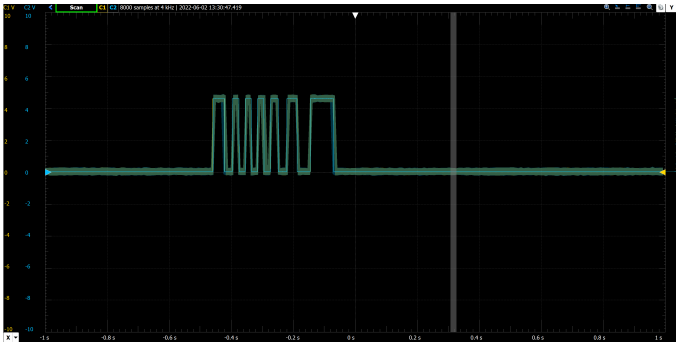

Fig. 15. Hall Effect Sensors Outputs for Phases A and C

VIII. Conclusion

The overall goal of constructing a functioning motor capable of moving a load as a proof of concept was achieved. To improve its performance, a couple of different steps could be taken. Firstly, the cogging behavior of the carriage as it travels along the bed can be reduced or entirely eliminated by improving the fitting. This would be done by sanding down the rails on the unibearing, tightening the carriage and applying wax to the bearing contact surface. Alternatively, a lower carriage design could have been employed to minimize the moment of torque as the carriage rotates slightly around the contact points.

Secondly, the bobbins would have to be redesigned and reprinted to have a channel that is wide enough to fit the hall effect sensors in their correct horizontal orientation about 5 mm above the magnet array. The ODrive would then need to be configured to keep the carriage within the bounds of the rail, and to correctly identify the switching of the magnetic phases as the carriage travels along the bed thereby allowing for more control of the positioning and movement of the carriage.

Refer here for STL files, detailed BOM, ODrive configuration commands, and FEMM simulation files used in this report.

Acknowledgment

The work presented here would not have been possible without support and feedback from Steven Clark, Aaron Goldin and Jason Poon. In addition to being great teachers throughout the quarter, they were great mentors and friends.

References

[1] D. Hitchins. (2022) When was the electric motor invented? a brief history of electric motors. [Online]. Available: https://www.parvalux.com/when-was-the-electric-motor-invented-a-brief-history-of-electric-motors/

[2] Aerotech. (2020) Linear motors: Application guide. [Online]. Available: https://www.aerotech.com/wp-content/uploads/2020/12/linear-motors-application-en.pdf

[3] Mainspring. (2022) Technology overview. [Online]. Available: https://www.mainspringenergy.com/technology/

[4] Instructables. (2020) Diy ironless linear servo-motor. [Online]. Available: https://www.instructables.com/DIY-IRONLESS-LINEAR-SERVO-MOTOR/

[5] B. Murphy. (2004) Design and construction of a precision tubular linear motor and controller. [Online]. Available: https://core.ac.uk/reader/4267990